Thin Solid Films 628 (2017) 208–213

Contents lists available at ScienceDirect

Thin Solid Films

journal homepage: www.elsevier.com/locate/tsf

$BaTiO_3$ thin films on platinized silicon: Growth, characterization and resistive memory behavior

A. Román [a,b], M. Rengifo [a,b], L.M. Saleh Medina [b,c], M. Reinoso [a,b,d], R.M. Negri [b,c], L.B. Steren [a,b], D. Rubi [a,b,d,*]

[a] Gereencia de Investigación y Aplicaciones, CNEA, Av. Gral Paz 1499 (1650), San Martín, Buenos Aires, Argentina
[b] Consejo Nacional de Investigaciones Científicas y Técnicas (CONICET), Argentina.
[c] Instituto de Química Física de Materiales, Ambiente y Energía (INQUIMAE) and Departamento de Química Inorgánica, Analítica y Química Física, Facultad de Ciencias Exactas y Naturales, Universidad de Buenos Aires, Buenos Aires, Argentina
[d] Escuela de Ciencia y Tecnología, UNSAM, Campus Miguelete (1650), San Martín, Buenos Aires, Argentina

ARTICLE INFO

Article history:
Received 11 October 2016
Received in revised form 8 February 2017
Accepted 17 March 2017
Available online 18 March 2017

Keywords:
Memristive oxides
$BaTiO_3$
Thin films on silicon

ABSTRACT

We report on the fabrication and characterization of Ti/$BaTiO_3$/Pt memristive devices. $BaTiO_3$ films were grown on platinized silicon by pulsed laser deposition with different laser pulse energies. We prove the existence of a correlation between the fabrication conditions and the microstructure and stoichiometry of the films. It is suggested that the small grain size found on our $BaTiO_3$ films destabilizes the structural tetragonal distortion and inhibits the appearance of long-range ferroelectric ordering. We show that even in absence of ferroelectric resistive switching (RS), two different RS mechanisms (metallic filament formation and oxidation/reduction of the Ti top electrode) compete, and can be selected by controlling the films stoichiometry and microstructure.

1. Introduction

The sustained increase of memory densities over the last decades has been, to a large extent, responsible for the remarkable evolution of micro- and nanoelectronics present in laptops, digital cameras, mobile phones, etc. Further progress, especially in portable appliances, crucially depends on the development of new solid-state memories. Today, dynamic random access memories (DRAM) and Flash represent the dominant memory technologies. DRAMs are fast and show almost unlimited cycle times for write and read operation, but they are volatile, i.e. they lose the stored information when the supply voltage is cut off. In addition, a further increase in storage density faces huge obstacles since their storage principle is charge-based. Although Flash memories are non-volatile and show better scaling potential than DRAMs, their write access is relatively slow and the number of write cycles is limited. The "holy grail" of the memory technology would be a RAM bringing together non-volatility, speed, durability and extended scaling. Different technologies have been proposed to accomplish these requirements, i.e. phase-change memories, magnetic or ferroelectric random access memories and resistive random access memories (RRAM). The latter are based on materials which show a significant, non-volatile, change in their resistance upon application of electrical stress, a mechanism that from early 00′s is usually called resistive switching (RS) (see reviews [1,2] and references therein). RS has been found to ubiquitously exist in a huge variety of simple and complex transition metal oxides. A typical RS device, usually called "memristor", consists in a metal/oxide/metal stack, usually laterally confined by means of standard micro or nanofabrication techniques. Although still immature compared to other approaches, RS materials show promising properties in terms of scalability, low power consumption and fast write/read access times. In addition, memristors were shown to exhibit a similar behavior than the bit-cells of the human brain (synapses) [3], suggesting the possibility of developing disruptive devices with neuromorphic behavior.

Up to now, the microscopic physical and chemical mechanisms underneath RS have not been fully understood. Different RS mechanisms have been proposed, being the most widely accepted related to the creation/disruption of conducting filaments bridging both electrodes, or to the drift-diffusion of oxygen vacancies that modulate the height of the Schottky barrier at the oxide/metal interface [1]. More recently, it has been proposed that in the case of ferroelectric oxides, the direction of the spontaneous polarization can also modulate the Schottky barrier at the oxide/metal interface, and therefore the device resistance [4–12]. These devices have the advantage of not relying on voltage-induced migration of ions -i.e. cations coming from the metallic electrode or oxygen vacancies- but on a pure electronic mechanism, being expected to display superior reliability and endurance.

Most reports on ferroelectric memristors deal with the room temperature multiferroic $BiFeO_3$ [6, 10–13] or with the canonical room

* Corresponding author at: Gerencia de Investigación y Aplicaciones, CNEA, Av. Gral Paz 1499 (1650), San Martín, Buenos Aires, Argentina.
E-mail address: rubi@tandar.cnea.gov.ar (D. Rubi).

http://dx.doi.org/10.1016/j.tsf.2017.03.038
0040-6090/

temperature ferroelectric $BaTiO_3$ (BTO) [4,5,7]. In the latter case, reports on epitaxial films grown on $SrRuO_3$ buffered $DyScO_3$ [14], $La_{2/3}Sr_{1/3}MnO_3$ buffered $NdGaO_3$ [7,15] or conducting Nb:$SrTiO_3$ substrates [16,17] can be found in the literature. In these cases, it is suggested that the ferroelectric character of the oxide layer plays a key role in the observed RS behavior. However, in order to allow a massive implementation of these devices, the growth of cheap, compatible metal oxide semiconductor (CMOS) devices on silicon is desired. A few works report on RS in polycrystalline $Ba_{0.6}Sr_{0.4}TiO_3$ thin films, grown either on platinized Si [18] or Ir/MgO/TiN buffered Si [19]. The RS found in these systems was reported to be independent of the ferroelectric properties of the oxide. In the first case, it was shown that the RS behavior is enhanced if the films are grown in Ar atmosphere, which increases the grain size and the existence of mobile oxygen vacancies. A similar RS scenario, related to the formation of oxygen vacancies filaments, is suggested in the second case. It is therefore worth asking if ferroelectric RS can be achieved in polycrystalline BTO thin films on buffered silicon. We recall that this is difficult task as a high control of the microstructure and the metal/oxide interfaces -usually rougher than in the case of epitaxial films- should be achieved in order to allow the stabilization of switchable ferroelectric ordering modulating the interface resistance.

In this article we study the memristive behavior of BTO thin films grown on platinized silicon by pulsed laser deposition under different growth conditions. The characterization of our samples suggests that in all cases the BTO films display a mixture of tetragonal and cubic phases. We propose that the small grain size of the films destabilize the tetragonal distortion and inhibits the appearance of long-range ferroelectric ordering. We show that even in absence of ferroelectric RS, two different resistive switching mechanisms -metallic filament formation and oxidation/reduction of the Ti top electrode- compete, and can be selected by tuning the films microstructure and stoichiometry. Alternative strategies for getting BTO-based heterostructures on Si with ferroelectric RS are discussed.

2. Experimental

BTO thin films were grown on (001) Pt/Ti/SiO_2/Si commercial substrates by pulsed laser deposition. A 266 nm Nd:YAG solid state laser, operating at a repetition frequency of 10 Hz, was used. The deposition temperature and oxygen pressure were 700 °C and 0.13 mbar, respectively. In order to modify the microstructure of the films we changed the energy per pulse of the laser beam between 50 and 100 mJ, maintaining the laser fluency constant at ~2 J/cm^2 by adjusting the area of the laser spot at the target position. X-ray diffraction was performed by means of an Empyrean (Panalytical) diffractometer. The film thickness was estimated by cross-section scanning electron microscopy imaging. Thicknesses of 390, 350 and 230 nm were obtained for films grown at 100, 70 and 50 mJ/pulse. The growth rates were estimated in 0.81, 0.32 and 0.15 Å/pulse, respectively. The microstructure of the films was observed by scanning electron microscopy (SEM), using a Carl Zeiss's Supra 40 microscope. Also, atomic force microscopy was performed in selected samples, by using a Veeco's Nanoscope III microscope to image the samples surface topography. Room temperature Raman spectra were recorded on a LabRAM HR Raman system (Horiba Jobin Yvon), equipped with two monochromator gratings and a charge coupled device detector (CCD). The Ar laser line at 514.5 nm was used as excitation source and it was filtered to give a laser fluence lower than 1 mW/mm^2 on the sample. 100 nm thick Ti top electrodes were deposited by sputtering and shaped by means of optical lithography. Top electrode areas ranged between 32×10^3 μm^2 and 196×10^3 μm^2. Electrical characterization was performed at room temperature with a Keithley 2612 source-meter hooked to a probe station. The bottom Pt electrode was grounded and the electrical stimulus was applied to the top electrode. Polarization versus applied electrical field loops were recorded at room temperature with a Radiant Precision LC Material Analyzer at a frequency of 1.5 kHz.

3. Results and discussion

Fig. 1 displays an X-ray diffraction pattern corresponding to a film grown with a laser pulse energy of 100 mJ. The spectrum suggests a polycrystalline growth, without any particular texture. Similar diffractograms were found in the cases of films grown at different pulse energies. The diffractogram was indexed by assuming the usual tetragonal room temperature structure [20], in spite of the fact that it has been reported that size effects present in polycrystalline films with reduced grain size can suppress the tetragonal distortion, leading to a cubic non-ferroelectric structure [21]. However, it should be pointed out that the typical full width half maximum (FWHM) of the diffraction peaks (typically 0.2–0.3°) is higher than the splitting expected between corresponding peaks of tetragonal and cubic BTO phases (for example, $\Delta(2\theta) = 0.1°$ between $(001)_T$ and $(100)_C$), indicating that this technique does not allow discriminating between these two structures. We will come back later to this issue. Mean crystallite size was estimated from peak (111) using the Scherrer equation, obtaining 93, 57 and 42 nm for 100, 70 and 50 mJ/pulse respectively. As can be seen, crystallite size increases with the energy per pulse.

Fig. 2 shows scanning electron microscopy images corresponding to films grown with laser pulse energies of 100 mJ ((a), (b)), 70 mJ ((c)) and 50 mJ ((d)). In the case of the films grown at the highest energy, a non-homogeneous microstructure with the presence of "cracks" is found. The distribution size of the grain follows a bimodal function centered at ~20 and ~80 nm. Upon lowering the laser energy, the microstructure becomes more homogeneous. In the case of the films deposited with 50 mJ pulses, only one type of grain with typical sizes below 20 nm is found. In all cases, a small amount of particulate, typical of pulsed laser deposition, [22] is found, covering less than 0.3% of the surface of the samples. The root mean square roughness values (RMS), derived from atomic force microscopy images (not shown here), are 3.49, 2.55 and 2.88 nm for films grown at 100, 70 and 50 mJ/pulse, respectively. The higher roughness obtained for the films grown at 100 mJ/pulse is related to the inhomogeneous microstructure of this film and to the presence of bigger grains. The Ba/Ti ratio was quantified by EDAX, obtaining values of 1.2, 1.1 and 1 for pulse energies of 50, 70 and 100 mJ, respectively. We recall that the expected ratio is $1 - \delta$, where δ depends on the thickness of the film and accounts for the contribution to the EDAX spectra of the adhesion Ti layer existing in

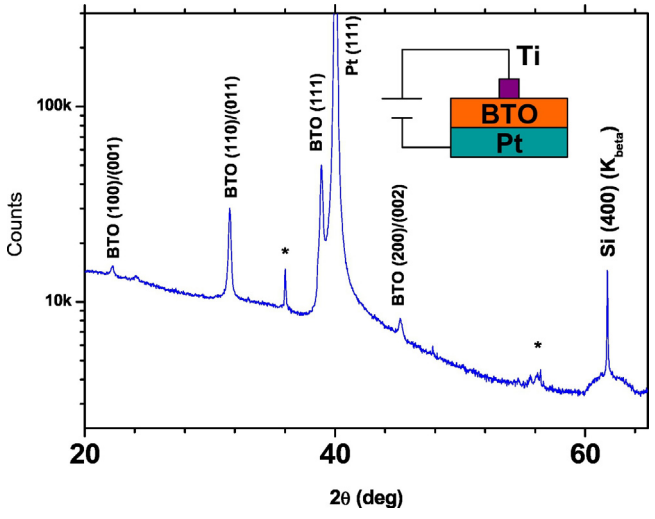

Fig. 1. X-ray diffraction pattern corresponding to a BTO/Pt/Ti/SiO_2/Si thin film. Peaks labeled with * correspond to a small amount of SiO_2 –buried below the Pt/Ti layers– that crystallizes during the BTO deposition process at high temperature. The inset shows a sketch of the connected device for electrical characterization.

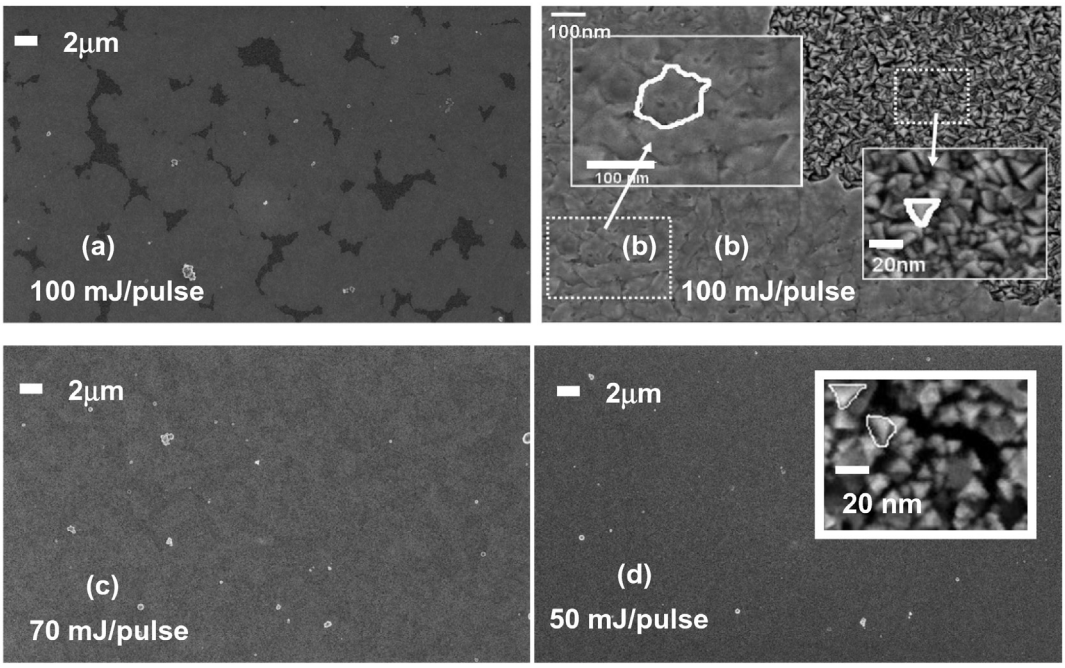

Fig. 2. Scanning electron micrographs corresponding to film grown at 100 mJ/pulse (a), (b), 70 mJ/pulse (c) and 50 mJ/pulse (d).

between the SiO_2 and Pt layers. The evolution of the deviation of the measured Ba/Ti ratio with respect to the expected (nominal) values for the different films is depicted in Fig. 3(b). The Ba excess increases as the laser energy decreases, indicating a higher ablation rate for Ba species for low pulse energies. This is likely related to an inhomogeneous laser beam, with zones where the fluence drops below the minimum energy threshold for congruent ablation [22]. The operation of the laser at 100 mJ/pulse leads to a more homogeneous beam, congruent ablation and a measured Ba/Ti ratio equal to the nominal one, within the technique resolution.

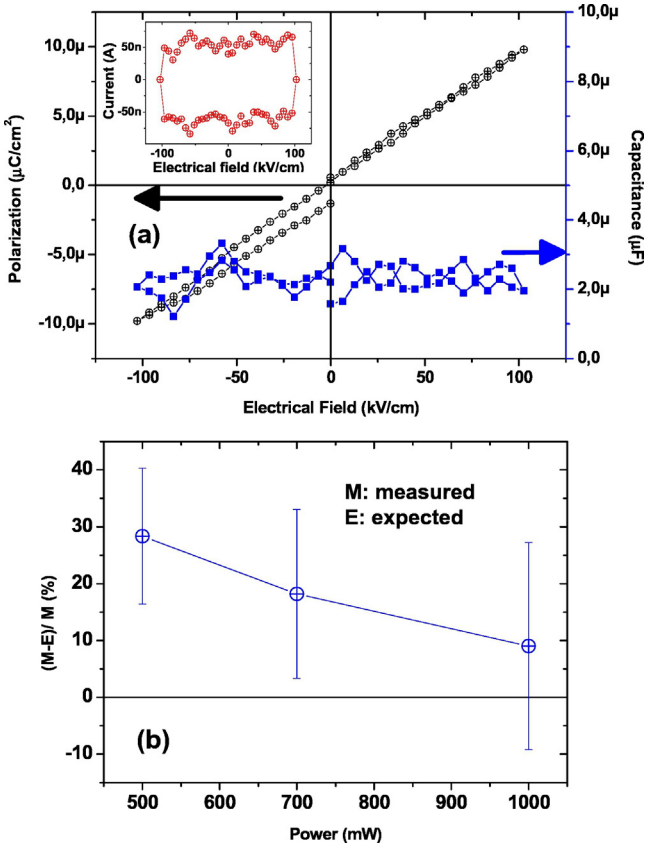

Fig. 3. (a) Polarization and capacitance as a function of the electrical field for a BTO/Pt device. The inset displays the leakage current for the same device. The lack of trend of the current with the electrical field is due to the rather low signal-to-noise ratio; (b) Evolution of the deviation of the measured Ba/Ti EDAX intensities with respect to the expected (nominal) values for films grown with different pulse energies.

Fig. 3(a) shows a typical polarization vs. electrical field loop recorded on a sample grown at 100 mJ/pulse. A linear non-hysteretic behavior is measured for this sample, indicating the absence of long-range ferroelectric ordering. We recall that the maximum applied electrical field (~100 kV/cm) is well above the reported coercive fields for submicrometric polycrystalline samples (<~5 kV/cm, according to Tan et al. [23]). The capacitance C, deduced from the polarization by taking into account that $C = dP/dV$, is constant, as expected for a linear capacitor. We remark that in the case of a ferroelectric capacitor the capacitance should display two sharp peaks at the coercive electrical fields. Measured leakage currents were below ~50 nA –see the inset of Fig. 3(a)–; these low values are consistent with the absence of the characteristic oval shape displayed by leaky samples [18,24]. A similar behavior was found for films grown at different pulse energies. Further information can be obtained by analyzing the relative permittivity, defined as $\varepsilon = C \times d / \varepsilon_0 \times A$, where d and A are the film thickness and the top electrode area, respectively. We have found values of 17, 25 and 31 for films grown at 50, 70 and 100 mJ/pulse, showing a monotonic increase with the pulse energy. We stress that typical values of permittivity for polycrystalline tetragonal BTO range between 80 and 1900 [25], indicating the presence of some amount of non-tetragonal phase with lower permittivity in our films [26]. According to these results, the films grown at 100 mJ/pulse are expected to present the highest amount of tetragonal phase.

In order to get further evidence about the crystalline phases present in our films, we have performed Raman spectroscopy, as shown in Fig. 4(a). The spectra display well defined features at 306, 520 and 714 cm^{-1}, that according to Parsons et al. [27] were classified as E (transverse), A (transverse) and mixed longitudinal modes, respectively. The E mode is a signature of the tetragonal phase, being absent in the Raman spectra of the cubic phase [27]. Interestingly, we found that the intensity of this mode increases monotonically with the energy per

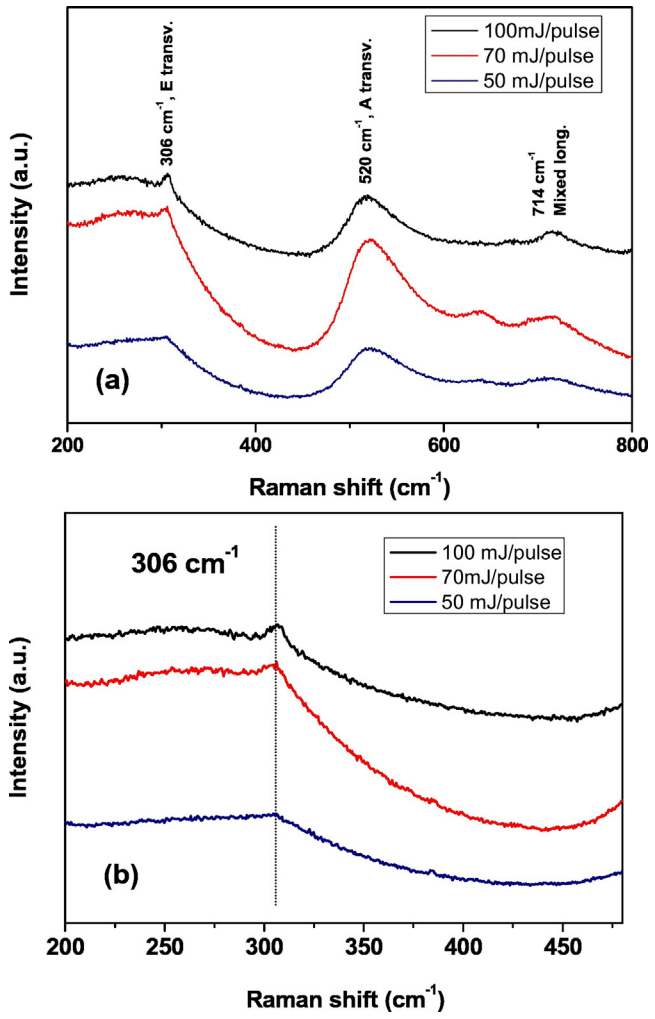

Fig. 4. (a) Raman spectra recorder for BTO films grown with different pulse energies; (b) blow-up of the spectra around 300 cm^{-1}, showing the progressive increase of the Raman E-mode as the pulse energy increases.

pulse used during the deposition, as shown in Fig. 4(b). This behavior strongly suggests that the formation of tetragonal phase is maximized for higher laser energies, consistently with the evolution of the permittivity described above. In consequence, based on the electrical and Raman characterization we propose a scenario where tetragonal and non-tetragonal (presumably cubic) phases coexist in our films. The amount of tetragonal phase is maximized for higher laser energy, but even in the case of films grown at 100 mJ/pulse the stabilization of a long-range ferroelectric ordering is not achieved. The formation of cubic phase can be related to the small grain size present in our samples as reported by Ring et al. [21].

We will focus now on the resistive memory behavior of the 100 and 50 mJ/pulse films. In the first case we found a virgin resistance of the order of a few MΩ, which is substantially different from the initial ~100 Ω found in the second case. We have recorded in both cases two types of measurements: pulsed current-voltage (I-V) curves and hysteresis switching loops (HSL). The pulsed I-V curve consists on applying a sequence of voltage pulses of different amplitude, with a time-width of a few milliseconds, while the current is measured *during* the application of the pulse. This is a dynamic measurement. Additionally, after the application of each of these pulses we apply a small reading voltage of 100 mV that allows us to measure the current and evaluate the *remnant* resistance state (HSL). Recorded I-V curves and HSLs for five consecutive cycles are displayed in Fig. 5 for both films. In the case of the 100 mJ/pulse film, it is found that the transition from high to low resistance (SET process) is found after the application of positive voltages in the range +1 V/+2 V, as shown in Fig. 5(a). The transition from low to high resistance states starts after the application of −0.8 V pulse and is gradual. The remnant resistance states can be observed in Fig. 5(b) and are in the range 500 kΩ/20 MΩ and 200 Ω/1 kΩ for high and low resistance states, respectively. This gives an average ON/OFF ratio of 5×10^6. The physical mechanism associated with the observed RS in this case can be related to the drift-diffusion of Ti atoms from the electrode to the oxide until a metallic nano-filament bridging both electrodes is formed. The application of positive (negative) stimulus to the top electrode induces the migration of Ti ions from the electrode and filament formation (retraction). The lack of dependence of the low resistance state with the top electrode area and the nearly ohmic behavior of this state (not shown here) support this scenario [1,28].

The behavior is completely different in the case of the 50 mJ/pulse films. Fig. 5(c) displays that the SET takes place for negative voltages (−1 V) and the RESET for positive stimulus (from +0.6 V), on the contrary of the 100 mJ/pulse film which displays the opposite I-V and HSL circulation. The high and low resistance states resulted ~1 kΩ and ~100 Ω, respectively, which gives an ON/OFF ratio of ~10 in this case. The dispersion found on SET voltages and remnant resistance values are substantially lower than in the case of 100 mJ/pulse films. The inset in Fig. 5(c) displays for both R_{HIGH} and R_{LOW} retention times of at least 500 s. Similar I-V curves were reported by Herpers et al. in manganite/Ti systems [29], and were attributed to the oxidation/reduction of a TiO_x layer formed at the Ti/manganite interface. This thin oxide layer is initially formed during the deposition of the electrode. A similar mechanism was proposed for $Ag/Ca_{0.1}Bi_{0.9}FeO_3$ system [30]. The application of positive voltage to the top electrode favors oxygen transfer between the oxide and the TiO_x layer, the latter increasing its oxygen content and therefore becoming more insulating. This is related to the observed RESET process observed with positive stimulus. The application of a negative stimulus reverses this process and gives place to the SET process. We propose that this mechanism dominates the RS behavior of our Ti/BTO structures when the oxide is deposited at low laser pulse energies (50 mJ/pulse). It is therefore worth asking about the physical property that controls the activation of the two RS mechanisms observed in both films. First, we should mention that the 100 mJ/pulse presents a less homogeneous microstructure, which should favor the migration of Ti ions through the cracks, defects and grain boundaries present in this sample. In this way, the filamentary regime stabilizes more easily and dominates the electrical behavior of the device. The more homogeneous microstructure of the 50 mJ/pulse film inhibits Ti migration [31] and unveils another dominant mechanism. In addition, we have shown that this film presents cationic off-stochiometries (Ba excess), which should enhance the conductivity of the BTO as it has been shown that A cations in excess in $ATiO_3$ oxides pair with oxygen vacancies and form n-type antisites defects, which increase the conductivity of the material [32]. This is related to the considerably lower virgin resistance found in this case. Upon the application of electrical stress, the low voltage drop on the BTO due to its low resistance allows a higher voltage drop at interface with the Ti electrode (TiO_x layer). This implies that a higher electrical field acts on the Ti/BTO interface and makes possible the oxidation/reduction of the interfacial TiO_x layer.

4. Conclusions

In summary, we have grown and characterized BTO thin films on platinized silicon. The microstructure of the films was demonstrated to be strongly dependent on the growth conditions. Moreover, we observe a coexistence of tetragonal and cubic crystalline phases correlated with the deposition conditions. The latter characteristic is associated with the small grain size of our films and is responsible for the absence of long-range ferroelectricity. Finally, a correlation between two

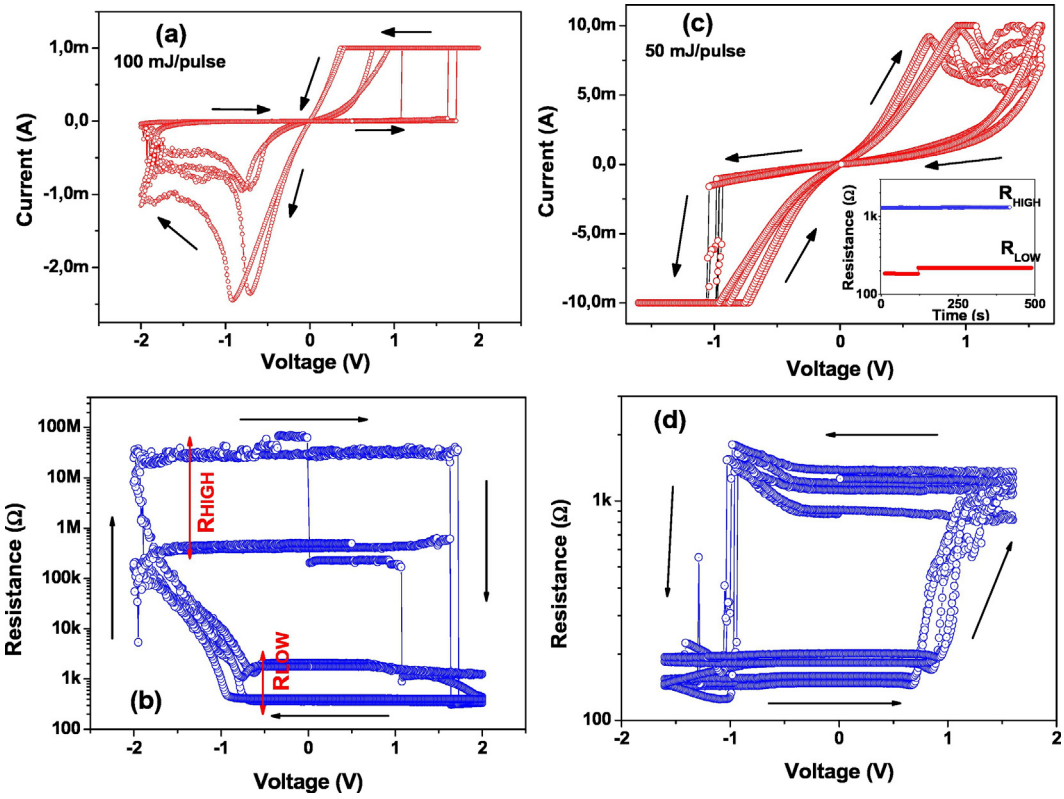

Fig. 5. (a), (b) Dynamic I-V curve and hysteresis switching loop corresponding to a Ti/BTO/Pt device, where the BTO layer was grown with a pulse energy of 100 mJ/pulse; (c), (d) same measurements for a 50 mJ/pulse film. The inset in (c) displays retention properties for both R_{HIGH} and R_{LOW} states of a 50 mJ/pulse film.

different RS mechanisms and the microstructure and stoichiometry of the films was disclosed. Future strategies to obtain ferroelectric RS in BTO-based structures on Si rely on the use of suitable buffers such as CeO_2/YSZ [33,34] to allow an epitaxial growth on Si.

Acknowledgement

We acknowledge financial support from CONICET (PIP 291), ANPCYT (PICT 2014-1047) and CIC-Buenos Aires. We thank Dr. D. Vega, from the Laboratory of X-ray Diffraction (GIA, GAIyANN, CAC, CNEA), for the XRD measurements.

References

[1] A. Sawa, Resistive switching in transition metal oxides, Mater. Today 11 (2008) 28.
[2] R. Waser, R. Dittmann, G. Staikov, K. Szot, Redox-based resistive switching memories — nanoionic mechanisms, prospects, and challenges, Adv. Mater. 21 (2009) 2632.
[3] Jo, et al., Nanoscale memristor device as synapse in neuromorphic systems, Nano Lett. 10 (2010) 1297.
[4] V. García, et al., Giant tunnel electroresistance for non-destructive readout of ferroelectric states, Nature 460 (2009) 81–84.
[5] A. Chanthbouala, et al., Solid-state memories based on ferroelectric tunnel junctions, Nat. Nanotechnol. 7 (2012) 101.
[6] A.Q. Jiang, et al., A resistive memory in semiconducting $BiFeO_3$ thin-film. Capacitors, Adv. Mater. 23 (2011) 1277.
[7] A. Chanthbouala, et al., A ferroelectric memristor, Nat. Mater. 11 (2012) 860.
[8] L. Wu, et al., Polarizatio-induced resistive switching behaviors in complex oxide heterostructures, Appl. Phys. Lett. 107 (2015) 122905.
[9] S. Kundu, Lead-free epitaxial ferroelectric material integration on semiconducting (100) Nb-doped $SrTiO_3$ for low-power non-volatile memory and efficient ultraviolet ray detection, Sci. Rep. 5 (2015) 12415.
[10] C.H. Yang, J. Seidel, S.Y. Kim, P.B. Rossen, P. Yu, M. Gajek, Y.H. Chu, L.W. Martin, M.B. Holcomb, Q. He, P. Maksymovych, N. Balke, S.V. Kalinin, A.P. Baddorf, S.R. Basu, M.L. Scullin, R. Ramesh, Electric modulation of conduction in multiferroic Ca-doped $BiFeO_3$ films, Nat. Mater. 8 (2009) 485.
[11] A. Tusumaki, H. Yamada, A. Sawa, Impact of bi deficiencies on ferroelectric resistive switching characteristics observed at p-type Schottky-like $Pt/Bi_{1-\delta}FeO_3$ interfaces, Adv. Funct. Mater. 22 (2012) 881.
[12] T. You, X. Ou, G. Niu, F. Bärwolf, G. Li, N. Du, D. Bürger, I. Skorupa, Q. Jia, W. Yu, X. Wang, O.G. Schmidt, H. Schmidt, Engineering interface-type resistive switching in $BiFeO_3$ thin film switches by Ti implantation of bottom electrodes, Sci. Rep. 5 (2015) 18623.
[14] Z. Wen, L. You, J. Wang, A. Li, D. Wu, Temperature-dependent tunneling electroresistance in $Pt/BaTiO_3/SrRuO_3$ ferroelectric tunnel junctions, Appl. Phys. Lett. 103 (2013) 132913.
[15] D.J. Kim, H. Lu, S. Ryu, S. Lee, C.W. Bark, C.B. Eom, A. Gruverman, Retention of resistance states in ferroelectric tunnel memristors, Appl. Phys. Lett. 103 (2013) 42908.
[16] Z. Wen, C. Li, D. Wu, A. Li, N. Ming, Ferroelectric-field-effect-enhanced electroresistance in metal/ferroelectric/semiconductor tunnel junctions, Nat. Mater. 12 (2013) 617.
[17] Z. Wen, D. Wu, A. Li, Memristive behaviors in $Pt/BaTiO_3/Nb:SrTiO_3$ ferroelectric tunnel junctions, Appl. Phys. Lett. 105 (2014) 052910.
[18] X. Yan, Y. Li, J. Zhao, Y. Li, G. Bai, S. Zhu, Roles of grain boundary and oxygen vacancies in $Ba_{0.6}Sr_{0.4}TiO_3$ films for resistive switching device application, Appl. Phys. Lett. 108 (2016) 033108.
[19] X. He, X. Li, Field-induced resistive switching of $(Ba_{0.6}Sr_{0.4})TiO_3$ thin films based on switching of conducting domains model, Appl. Phys. Lett. 102 (2013) 221601.
[20] Shizuo Miyake, Ryuzo Ueda, On phase transformation of $BaTiO_3$, J. Phys. Soc. Jpn. 2 (93) (1947).
[21] K.M. Ring, K. Kavanagh, Substrate effects on the ferroelectric properties of fine-grained $BaTiO_3$ films, J. Appl. Phys. 94 (2003) 5982.
[22] Douglas B. Chrisey, Graham K. Hubler, Pulsed Laser Deposition on Thin Films, John Wiley & Sons, New York, 1994.
[23] Y. Tan, J. Zhang, Y. Wu, C. Wang, V. Koval, B. Shi, H. Ye, R. McKinnon, G. Viola, H. Yan, Unfolding grain size effects in barium titanate ferroelectric ceramics, Sci. Rep. 5 (2015) 9953.
[24] Haixue, et al., The contribution of electrical conductivity, dielectric permittivity and domain switching in ferroelectric hysteresis, J. Adv. Dielectrics 1 (2011) 107.
[25] Jin Wook Jang, Su Jin Chung, Woon Jo Cho, Taek Sang Hahn, Sang Sam Choi, Thickness dependence of room temperature permittivity of polycrystalline $BaTiO_3$ thin films by radio-frequency magnetron sputtering, J. Appl. Phys. 81 (1997) 6322.
[26] Q.X. Jia, Z.Q. Shi, W.A. Anderson, $BaTiO_3$ thin film capacitors deposited by r.f. magnetron sputtering, Thin Solid Films 209 (1992) 230.
[27] J.L. Parsons, L. Rimai, Raman spectrum of $BaTiO_3$, Solid State Commun. 5 (1967) 423.
[28] D. Rubi, F. Tesler, I. Alposta, A. Kalstein, N. Ghenzi, F. Gomez-Marlasca, M. Rozenberg, P. Levy, Two resistive switching regimes in thin film manganite memory devices on silicon, Appl. Phys. Lett. 103 (2013) 163506.

[29] A. Herpers, C. Lenser, C. Park, F. Offi, F. Borgatti, G. Panaccione, S. Menzel, R. Waser, R. Dittmann, Spectroscopic proof of the correlation between redox-state and charge-carrier transport at the interface of resistively switching Ti/PCMO devices, Adv. Mater. 26 (2014) 2730.
[30] D. Rubi, F.G. Marlasca, M. Reinoso, P. Bonville, P. Levy, Magnetism and electrode dependant resistive switching in Ca-doped ceramic bismuth ferrite, Mater. Sci. Eng. B 177 (2012) 471.
[31] D. Rubi, et al., Manganite based memristors: influence of the electroforming polarity on the electrical behavior and radiation hardness, Thin Solid Films 583 (2015) 76.
[32] C. Lenser, A. Koehl, I. Slipukhina, H. Du, M. Patt, V. Feyer, C.M. Schneider, M. Lezaic, R. Waser, R. Dittmann, Formation and movement of cationic defects during forming and resistive switching in $SrTiO_3$ thin film devices, Adv. Funct. Mater. 25 (2015) 6360.
[33] D. Rubi, S. Duhalde, M.C. Terzzoli, G. Leyva, G. Polla, P. Levy, F. Parisi, R.R. Urbano, Structural and electrical characterisation of $La_{0.5}Ca_{0.5}MnO_3$ thin films grown by pulsed laser deposition, Phys. B 320 (2002) 86.
[34] M. Scigaj, N. Dix, I. Fina, R. Bachelet, B. Warot-Fonrose, J. Fontcuberta, F. Sánchez, Ultra-flat $BaTiO_3$ epitaxial films on Si(001) with large out-of-plane polarization, Appl. Phys. Lett. 102 (2013) 112905.